O'CONNELL: Do I understand you to say that the shortest orbital period you have found is of the order of 500 days?

LLOYD EVANS: Yes.

PERCY: Since it is known that there are non-variable stars in the Cepheid instability strip, it may be possible that the presence of a „close" companion may inhibit pulsation, and thereby explain the absence of short-period orbital motion among Cepheids.

LLOYD EVANS: The shortest orbital period for a non variable F-G supergiant binary is about 200 days. The stars selected by spectral type form a less well defined group than classical Cepheids, so it seems likely that this is a little less massive and post red-giant tip. Cepheids in binaries do not seem to differ significantly from single Cepheids in their pulsation properties or otherwise.

FERNIE: I think the question of the repeatibility of Cepheid light- and velocity-curves is one which needs careful investigation. There are at least some Cepheids, e. g. SV Vul, in which the scatter of observed points determined in different cycles becomes significantly greater at certain phases. This is important both in itself and from the standpoint of WESSELINK radii.

LLOYD EVANS: I would like to stress the importance of intensive photoelectric observation of selected Cepheids to establish the repeatability of their light curves.

MAVRIDIS: I would like to point out that TSIOUMIS and myself have observed the Cepheids X Lac, RR Lac, Z Lac, U Vul, and CD Cyg during the years 1967—1970 using 2 comparison stars for each Cepheid. In this way very accurate and detailed light- and colour-curves (UBV system) have been obtained. The same Cepheids were observed also by BAHNER and myself in 1956—59 using the same comparison stars (BV system). A comparison of the light and colour-curves corresponding to these 2 observational series show that the light- and colour-curves of X Lac and CD Cyg show changes between the 2 series. The light- and colour-curves of RR Lac, Z Lac and U Vul on the contrary do not show any significant changes between the 2 observational series.

The Spectrum Variable a Centauri (HD 125 823)

D. A. KLINGLESMITH and P. L. BERNACCA*) (NASA, Goddard Space Flight Center Greenbelt) and H. FREY (College Park, Maryland)

Abstract

High dispersion spectra in the blue violet region and OAO II spectral scans in the UV of the star a Centauri are presented. The variation of equivalent widths and radial velocity are presented. The appearance and disappearance of the forbidden lines of helium, the change in the wing structure of λ 4471 of HeI, the strengthening of the UV resonance lines at phase 0.5 and the presence of the UV feature of λ 1720 indicate that the star's atmosphere is experiencing drastic density changes.

I. Introduction

The star a Centauri is unique in that the helium absorpion line spectrum varies in strength by at least a factor of 10 with an 8.8 day period while the other spectral features either change by a factor 2 or don't change at all (NORRIS 1968, 1971; JASCHEK, JASCHEK and KUCEWICZ 1968; and JASCHEK, JASCHEK, MORGAN and SLETTEBAK 1968). This paper will present the analysis of a series of high resolution spectra in the blue-violet spectral range

*) ESRO Associate 1971 on leave from Asiago Observatory, Italy.

https://doi.org/10.1017/S0252921100032978 Published online by Cambridge University Press

taken by Dr. Anne B. UNDERHILL and a series of UV spectral scans obtained by Dr. M. R. MOLNAR with the Wisconsin Experiment Package aboard OAO-II. The spectral variations are complex in that several different types of variation exist, all with the same 8.8 day period. It will be suggested that density variations in the atmosphere could explain the observations. However, it is not yet possible to determine whether they are due to pulsation, tidal distortion or a rotating partial shell.

II. The Visual Spectra

The blue-violet spectra were obtained with the Coudé-spectrograph of the 1.5 meter telescope of the European Southern Observatory in Chile by Dr. UNDERHILL. The spectra were obtained on Kodak IIaO plates with a dispersion of 3.3 Å/mm and covered the spectral range from λ 3500 Å to λ 4900 Å. Table I lists the date, time, length of exposure and phase (using the epoch and period determined by NORRIS, 1971).

Table 1: Photographic Data for a Centauri

Plate	Date (1970)	Time (UT)	Duration	Phase
H 131	June 9	0^h33^m	3^h17^m	0.223
132	10	23^h50^m	$2^h\ 0^m$	0.447
136	12	23^h28^m	1^h31^m	0.673
143	22	0^h18^m	$3^h\ 0^m$	0.697
148	23	23^h28^m	1^h20^m	0.921
150	24	23^h21^m	1^h10^m	0.033

Table 2: Measured equivalent widths

λ	Element ion.	#	Plate Phase	H150 0.03	H131 0.22	H132 0.45	H136 0.67	H143 0.69	H148 0.92
3805.567	He I	63		15	35				
3806.56	Si III	5		60	86	75	83	92	54
3819.606									
3819.670	He I	22			699		649	1054	1600
3853.657	Si II	1		50	43	42	47	44	44
3856.021	Si II	1		92	89	91	83	76	100
3860.650	S III	5				13	39	23	
3862.592	Si II	1		91	75	63	83	60	92
3867.477									
3867.631	He I	20		497	171	23	123	82	245
3876.188	C II	33		109	57	98	98	92	82
3918.977	C II	4		90	134	100	108	103	95
3920.677	C II	4		109	111	99	104	116	116
3924.440	Si III				34	48	71	55	
3926.550	He I	58		967	844		61	183	881
3933.664	Ca II	1		123	165	122	103	77	120
3945.048	O II	6						24	41
3954.372	O II	6		54	32	40	39	29	78
3955.851	N II	6			47	32	26	18	25

https://doi.org/10.1017/S0252921100032978 Published online by Cambridge University Press

λ	Element ion.	#	Plate Phase	H150 0.03	H131 0.22	H132 0.45	H136 0.67	H143 0.69	H148 0.92
3964.727	He I	5		180	61		70	66	152
3970.074	H 7			6761	6601	5590	6535	6049	6805
3994.996	N II	12		48	63	103	74	63	49
4005.040	Fe III	45					39	24	
4009.270	He I	55		1118	596	81	304	347	1007
4026.189	He I	18		2226	1189	262	1416	930	2008
4035.09	O II	51			30	37	40	18	36
4041.321	N II	39		22	26	49	32	39	22
4043.537	N II	39		17		47	24	31	
4069.636									
4069.897	O II	10		55	71	49	51	43	71
4072.164	O II	10		29	60	30	32	43	57
4074.530	C II	36		30	47	28	43	29	27
4075.868	O II	10		71	100	71	78	63	87
4101.737	H 6			5999	5819	5263	6007	5719	6476
4119.227	O II	20			40	49	24		
4120.819									
4120.993	He I	16		342	224	74	215	193	294
4122.93	Fe III	118			28		36	38	
4128.053	Si II	3		49	75	68	66	82	61
4130.884	Si II	3		56	81	60	84	60	71
4143.759	He I	53		1469	753	53	345	260	1381
4150.302	Al III	5			36	16	17	53	
4153.098	S II	44		71	49	41	28	37	61
4164.79	Fe III	118				51	36	34	53
4166.86	Fe III	118					25	27	
4168.971	He I	52		172	53		28	55	192
4174.042	S II	64			15				41
4185.456	O II	36		19	39		12		
4189.778	O II	36		38	36		28	38	33
4222.15	P III	3		23	23	25		18	17
4227.749	N II	33				20		19	21
4233.169	Fe II	27				18			17
4236.930	N II	48		17	38	36		43	13
4241.787	N II	47		39	17	31		35	19
4267.020									
4267.270	C II	6		176	183	207		224	223
4317.139	O II	2		40		40		34	28
4319.631	O II	2		21		30		23	23
4340.468	H 5			6197	5590	5167		5026	5335
4349.690	O II	2		16	10	21		27	
4372.490	C II	45		49		47		59	
4374.28	C II	45		13		20		16	14
4384.643	Mg II	10			40			12	12
4387.929	He I	51		1193	654	64		304	873
4390.585	Mg II	10			16	30		31	11
4411.520	C II	39		35		39		34	13
4414.909	O II	5		27	55	25		37	31
4416.975	O II	5		23	34	25		36	9
4432.410	S II	43		15		23		10	

https://doi.org/10.1017/S0252921100032978 Published online by Cambridge University Press

λ	Element ion.	#	Plate Phase	H150 0.03	H131 0.22	H132 0.45	H136 0.67	H143 0.69	H148 0.92
4437.549	He I	50		194	62			39	134
4447.033	N II	15		34	41	33		20	21
4471.477	He I	14		1849	1294	261		593	1621
4479.968	Al III	8		24		16		21	24
4481.129									
4481.327	Mg II	4		191	211	162		170	201
4512.535	Al III	3		21		5		16	20
4524.946	S II	40							
4528.911	Al III	3		40	46	35		36	41
4530.403	N II	59		22		54		15	6
4549.467	Fe II	36		16		18		29	18
4552.654	Si III	2		88	95	94		111	85
4567.872	Si III	2		68	73	75		103	89
4574.777	Si III	2		32	46	48		65	42
4590.971	O II	15		11	9	30		14	13
4596.300	O II	15		16	18	20		23	9
4602.75	Fe II	19		18		32		26	17
4607.153	N II	5			27	37		34	15
4613.868	N II	5		11	22	48		40	18
4621.392	N II	5		11	23	45		50	17
4630.537	N II	5		31	42	72		59	40
4638.854	O II	1		17		30		35	18
4641.811	O II	1		20	27	23		37	26
4643.086	N II	5		17	24	34		44	17
4649.139	O II	1		40	48	41		61	25
4650.840	O II	1		19	21	23		34	21
4676.234	O II	1		43		18		35	25
4713.143									
4713.373	He I	12		338	148	48		148	284
4810.280	N II	20				17		36	18
4815.515	S II	9		62	45	36		21	55
4813.290	Si III	9			27	29		20	
4819.740	Si III	9		35		71		66	65

Figure 1 presents 2 regions of the spectra that show the extremes of the helium absorption line variation. Figure 1 (a) shows the region near H_ϵ. The He I singlet λ 3926.534 (2^1P°—8^1D) is seen as a broad shallow line near zero phase and is completely absent at phases near 0.5. The other He I singlet λ 3964.729 (2^1S—4^1P) is also strong near zero phase and absent near phase 0.5. In contrast the Si III line λ 3924.44, the O II lines $\lambda\lambda$ 3945.048, 3954.372 ($3s^2P$—$3p^2P^\circ$) and the N II line λ 3994.996 ($3s^1P^\circ$—$3p^1D$) vary in anti-phase to the helium lines, but not by nearly so great a factor. The CaII K line λ 3933.664 (4^2S—4^2P°) does not appear to vary. Figure 1 (b) presents another region of the spectrum. The triplet line of He I λ 4471.688, .477 (2^3P°—4^3D) varies from a very strong line with broad wings and a sharp core at zero phase to only a sharp core near phase 0.5. The forbidden line of He I λ 4469.92 (2^3P°—4^3F°) appears and disappears in phase with the other He I line variations. The presence of the forbidden line usually implies a high density atmosphere and its absence and the lack of wings on λ 4471 implies a low density atmosphere. The Mg II line λ 4481.129, .327 (3^2D—4^2F°) has an equivalent width variation of 20 percent or less and is in phase with the He I line variations.

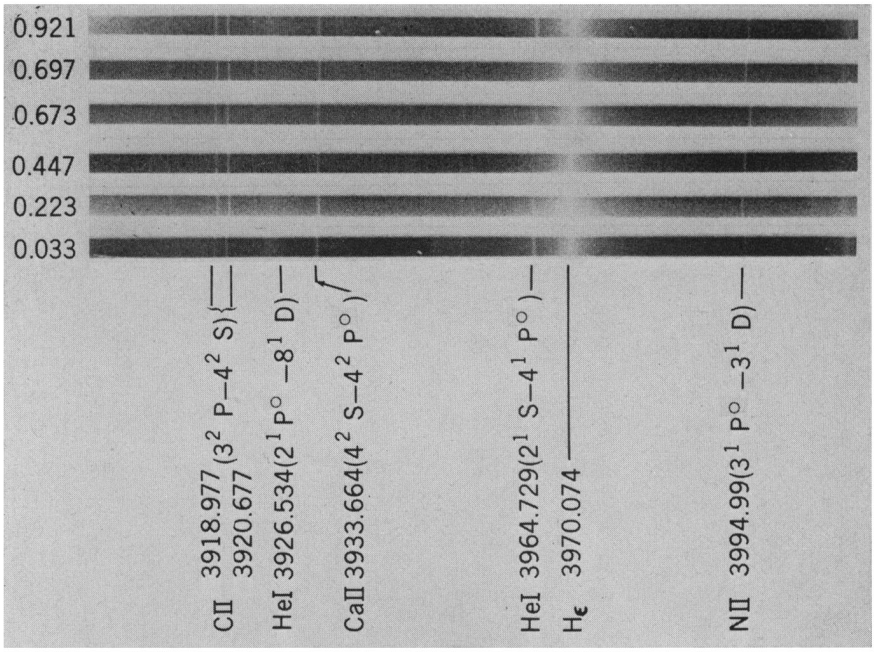

Fig. 1a: The spectra of a Cen as a function of phase — the region near H_ϵ. The phase is indicated alongside each spectra and the lines are identified in the standard way.

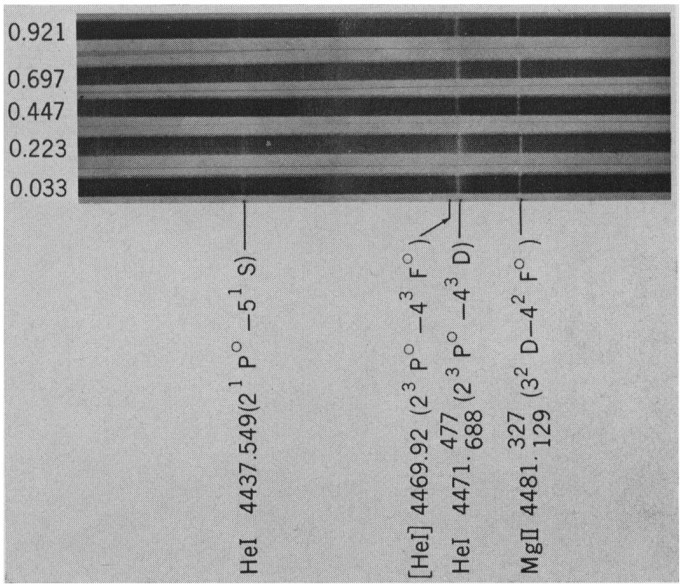

Fig. 1b: The spectra of a Cen as a function of phase — the region near Mg II 4481.

https://doi.org/10.1017/S0252921100032978 Published online by Cambridge University Press

Table 3: Possible Contributions to the Prominent Absorption Features

Position Wavelength Å	Possible Contributors	Multiplet	Wavelength Å
1720	Mn II	13	1734—1738
	Cr IV	14	1731
	Si IV	10	1722—1727
	C II	14.02	1720—1722
	Al II	6	1719—1725
	N IV	7	1719
	Cr III	34	1712, 1720
	Fe II	37, 38, 39	1710—1725
	Ni II	4	1710
	S I	10	1706, 1707
	Si II	10, 10.01	1705—1711
	Ni III	15, 16, 25, 28, 30, 31	1702—1739
1478	Sr II	7	1483—1489
	S I	3, 4	1474—1487
	Si II	12, 12.01, 12.02, 15.04	1474—1485
	Ni II	6	1468
	Ti IV	3	1467, 1469
1399	Si II	13.02, 13.03, 14	1404—1410
	Si IV	1	1394, 1403
	Cl I	1	1390—1397
	S I	6, 7	1386—1413
	Mn II	14	1386
	Cr III	35	1384—1400
1334	Ca II	2	1342
	Cl I	2	1336—1352
	P III	1	1335—1345
	C I	4	1329—1330
	Ti III	4	1328
	C II	1, 11	1324—1336
	S I	8	1324, 1327
	N I	11, 12	1319—1328

Density tracings of each spectra were recorded on magnetic tape with a Joyce-Loebl microdensitometer and converted to intensity in the computer with wavelength dependent HD curves. The intensity traces were plotted on a wavelength scale using the strong lines (other than hydrogen) to determine a quadratic relation between date point number and wavelength. The accuracy of this procedure was such that the wavelength of a feature could be determined to $\pm$ 0.1 Å. All absorption features were identified and equivalent widths (W_λ) for each feature were obtained. It was possible to measure features that had $W_\lambda \geq 0.02$ Å. The wavelength identification and W_λ for each feature as a function of phase is given in Table II. Figures 2—6 show the variation of some equivalent widths that were measured. If we consider the He I variation to be the primary variation then the hydrogen lines vary in phase with the helium lines (Figure 2). The Si II (1) lines vary almost in phase whereas the Si II (3) lines do not vary (Figure 3). In Figure 4 the Si III (2) lines vary in anti-phase with the Si II (1) lines. The other Si III lines tend to agree with that variation. In Figure 5 all of the N II lines vary in anti-phase with the He I lines. Figure 6 shows the Mg II and P III do not vary but that the Ca II line does seem to vary in phase with the helium lines or more likely in phase with the Si II (1)

https://doi.org/10.1017/S0252921100032978 Published online by Cambridge University Press

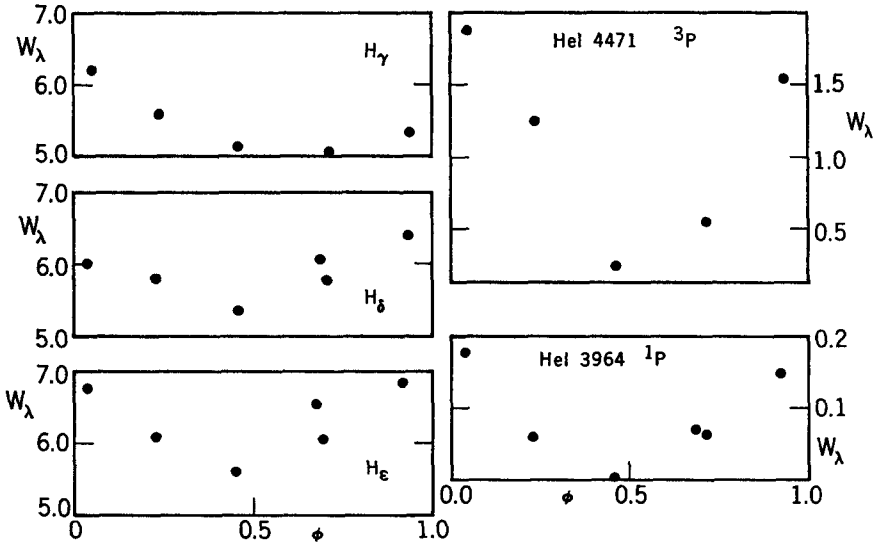

Fig. 2: The equivalent width variation of 3 hydrogen lines and 2 helium lines as a function of phase.

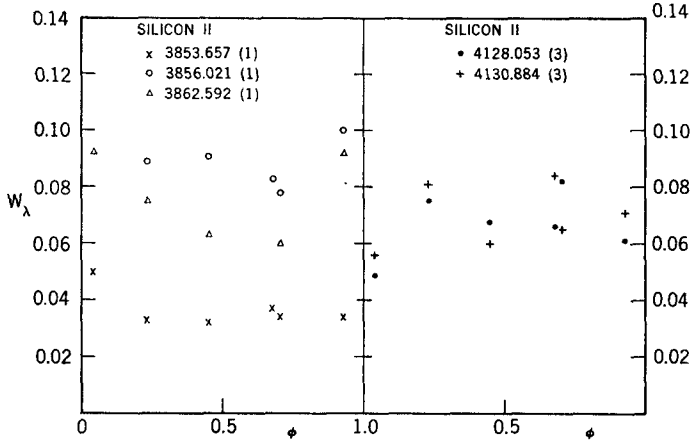

Fig. 3: The equivalent width variation of Si II line.

https://doi.org/10.1017/S0252921100032978 Published online by Cambridge University Press

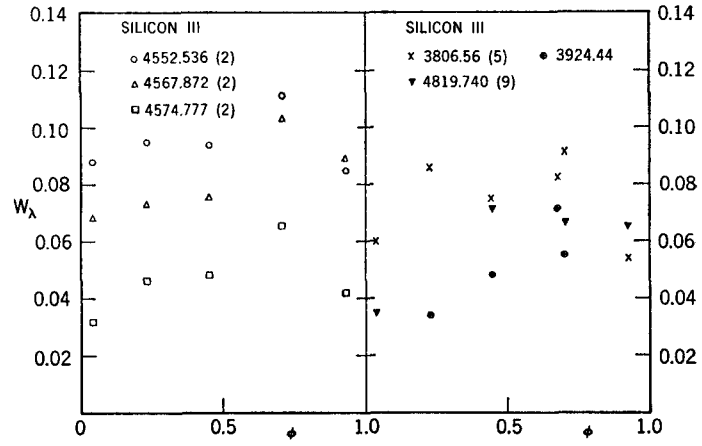

Fig. 4: The equivalent width variation of Si III lines.

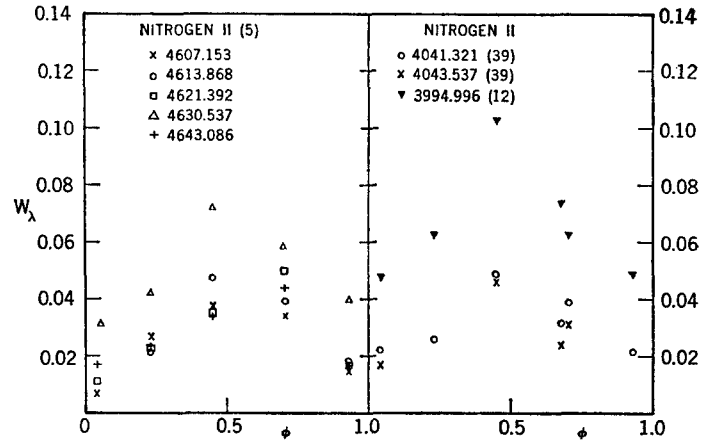

Fig. 5: The equivalent width variation of N II

https://doi.org/10.1017/S0252921100032978 Published online by Cambridge University Press

lines. Figures 2—6 point out some of the complexity of the variations that must be explained by any model for this star.

Besides equivalent widths, the radial velocities of the various strong lines were measured using a Grant comparator. Figure 7 shows the results for hydrogen and helium. The points for hydrogen at each phase are the average of 6 lines from $H\gamma$ to H10. The helium lines have been separated into singlets and triplets. The singlets used were 4437, 4387, 4168, 4143 and 3964; the triplets used were 4713, 4471, 4120, and 4026. The error bars in the figure show the standard deviation of the average. The radial velocity of hydrogen appears to vary in phase with the W_λ of He I. However, the radial velocity of the triplets of helium does not vary while the radial velocity of the singlets, when measurable, appears to vary in anti-phase with the radial velocity of hydrogen. Figure 8, 9 and 10 show that the radial velocity of the metal lines varies in phase with that of hydrogen.

III. The Ultraviolet Spectrum

Eleven UV spectra of a Centauri obtained by Dr. M. R. MOLNAR using the Wisconsin experiment package on board OAO-II are shown in Figure 11. The logarithm of the count rate is plotted as a function of grating step. Each grating step represents a 10 Å bandpass. The flux level of a Centauri is such that it required 2 scans to be added together in order to obtain significant count levels. The stronger features are indicated in the same manner as UNDERHILL, LECKRONE and WEST (1972). The lines that might be contributing to each major feature are listet in Table 3. These major features all seem to vary in anti-phase with the He I lines, i. e. large „equivalent width" at phases near 0.5 and small near zero phase. Their predominant contributions are Si III, Si IV, C III and P III.

The UV scans of a Centauri have been compared with other raw data from OAO-II (LECKRONE — unpublished) of stars with similar small reddening. The closest agreement is to be found with β Cep (B 2 III), β CMa (B 1 III) and ϑ Oph (B 2 IV) all of which are β CMa variables.

The feature at 1720 Å has been found in all supergiants and most shell stars observed with OAO-II (UNDERHILL, LECKRONE and WEST 1972). It is not as strong in a Centauri as in supergiants. Nevertheless it certainly is an indication that the density in the atmosphere is less around phase 0.5 than at other phases, which is in agreement with the line strength variation in both the visual and ultraviolet region.

IV. Conclusion

The appearance and disappearance of the forbidden line of He I λ 4469.92, and the change in the very structure of 4471 of He I, the strengthening of N III λ 3995, the strengthening of the UV resonance lines at phase 0.5, and the presence of the UV feature at 1720 Å seen in a Centauri indicate that by some manner, as yet unexplained, there is a change from a dwarf type spectrum at zero phase to a giant type spectrum at phase 0.5. The lack of change of the continuum slope in the ultraviolet indicates that there is not a significant temperature change in the atmosphere.

Acknowledgements

This work has been partially supported by a post-doctoral fellowship to P. L. BERNACCA by the European Space Research Organization. Dr. Marshall GINTER of the Molecular Physics Institute of the University of Maryland is gratefully acknowledged for permission to use the grant comparator.

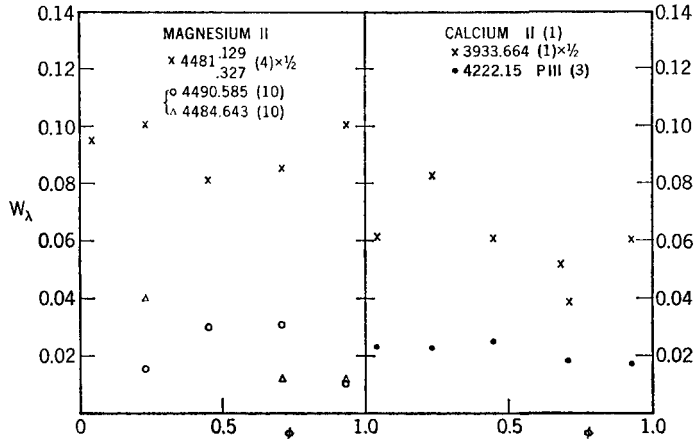

Fig. 6: The equivalent width variation of Mg II, Ca II and P III lines.

References:

JASCHEK, M., JASCHEK, C., and KUCEWICZ, B., **1968**, Nature, **219**, 1137.
JASCHEK, C., JASCHEK, M., MORGAN, W. W., and SLETTEBAK, A., **1968**, Ap. J. Letters, **153**, L87.
NORRIS, J., **1968**, Nature, **219**, 1342.
NORRIS, J., **1971**, Ap. J. Suppl., **23**, 235.
UNDERHILL, A. B., LECKRONE, D. S., and WEST, D. K., **1972**, Ap. J. in press.

Discussion to the paper of KLINGLESMITH, BERNACCA and FREY

RAKOŠ: What is the dispersion of your spectrograms?

KLINGLESMITH: 3.3 Å/mm.

PERCY: Would you please comment on the suggestion that the variations in this star (and also in the β Cep, which you discussed earlier at this conference) are due to the slow rotation of a star with a „spot". The periods of this star and of β Cep are reasonable for stars of low v sin i.

KLINGLESMITH: The idea of a helium rich spot is hard to defend in the light of the obvious pressure effects on the He I and N II lines.

DE GROOT: Is there an identification for the λ 1720 Å line and would you, please, say something about the accuracy of your equivalent width measurements; many of your variable lines are weaker than 100 mÅ.

KLINGLESMITH: The 1720 feature is probably due to a blend of Ni II and Ni III lines. The equivalent widths are accurate to $\pm$ 20%.

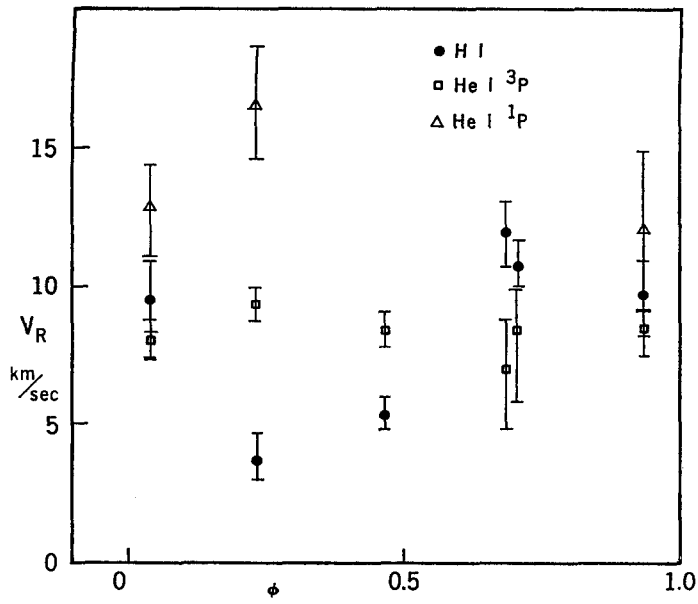

Fig. 7: The radial velocity variations of hydrogen and helium. The helium singlets and triplets have been separated to show the difference in behaviour.

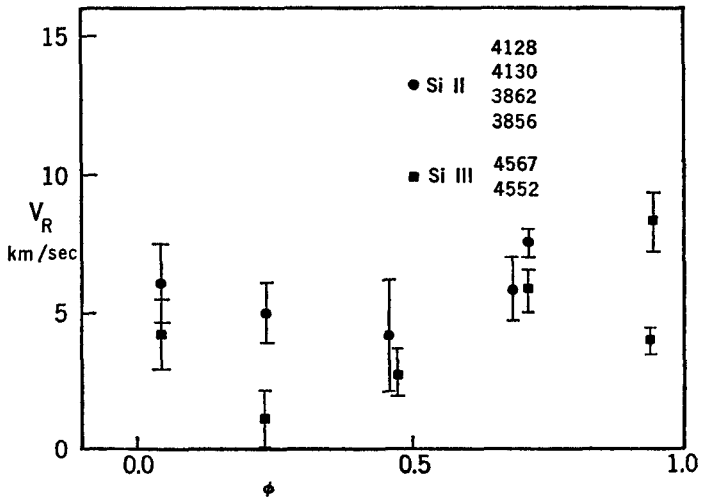

Fig. 8: The radial velocity variation of Si II and Si III lines.

https://doi.org/10.1017/S0252921100032978 Published online by Cambridge University Press

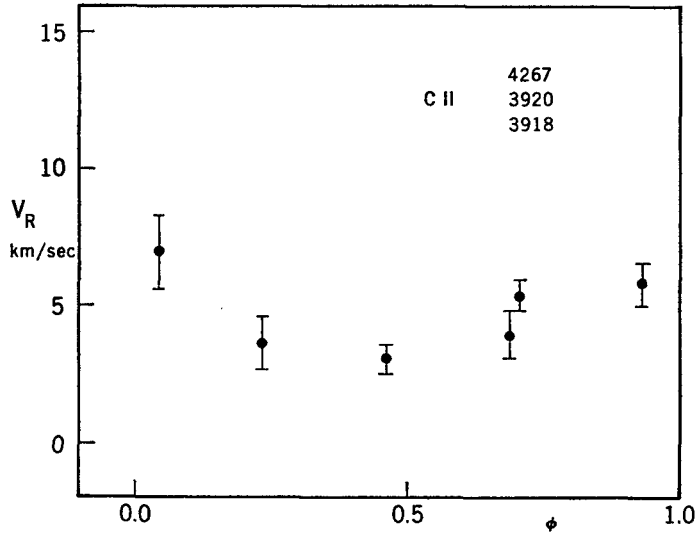

Fig. 9: The radial velocity variation of C II lines.

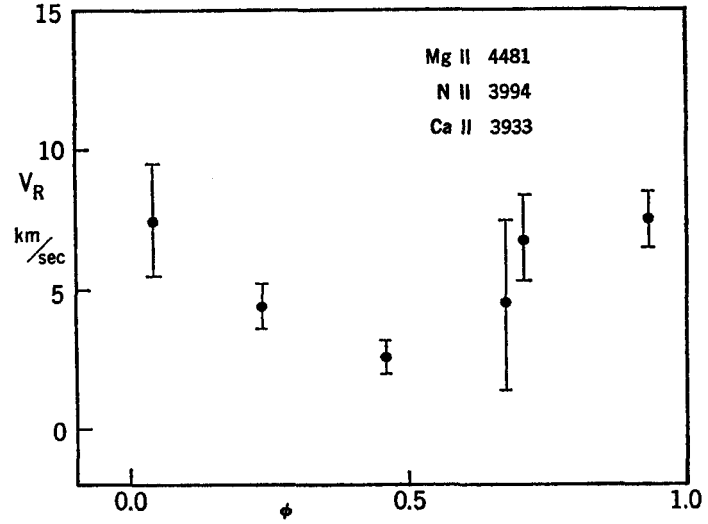

Fig. 10: The average of the Mg II, N II and Ca II radial velocity variations.

https://doi.org/10.1017/S0252921100032978 Published online by Cambridge University Press

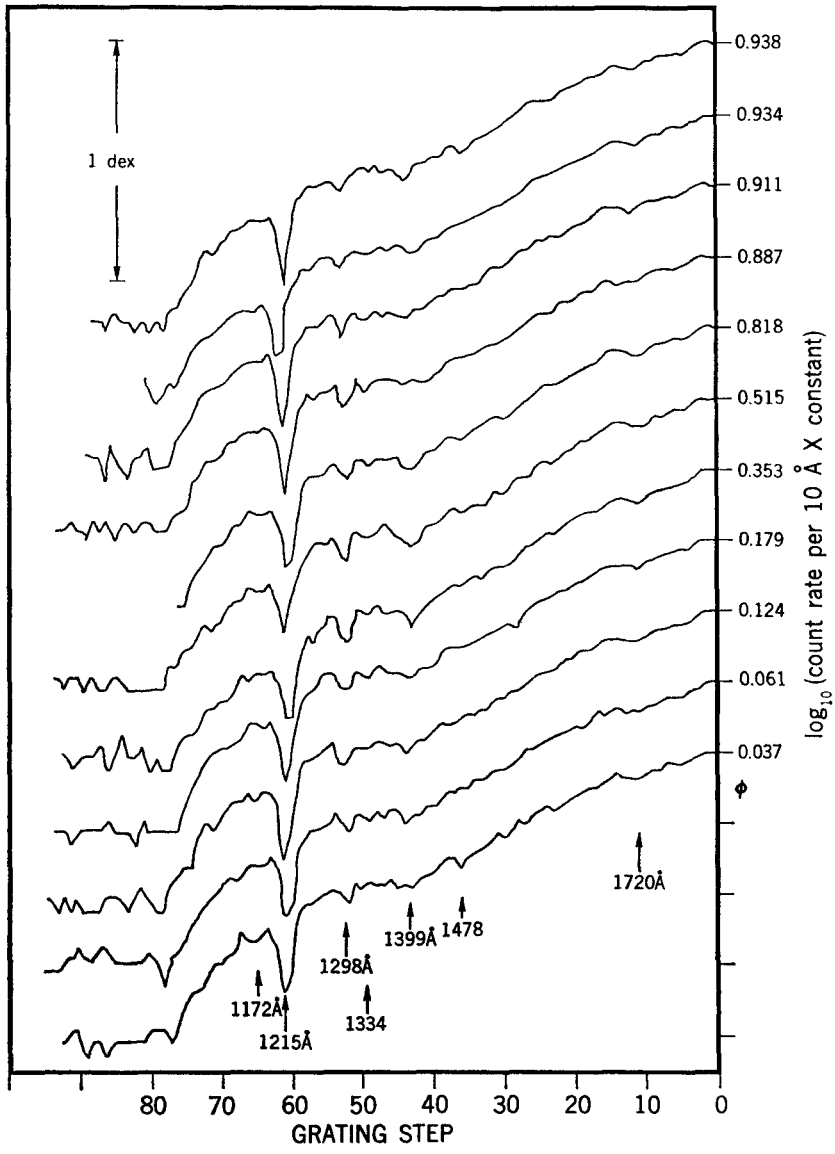

Fig. 11: The UV scans from OAO-II of a Centauri as a function of phase. The strong features labeled are listed in Table 3 with their major contributors.

https://doi.org/10.1017/S0252921100032978 Published online by Cambridge University Press